strate here that p53 uses a palindromic binding site to regulate its target gene *PAC1*. Thus, it is conceivable that p53 may selectively regulate different groups of target genes through this mechanism or through conventional mechanisms. The identification of this mechanism for p53 action will provide insights into the molecular basis of how p53 selectively regulates its target genes to eliminate cancer cells and suppress tumorigenesis. □

Methods

Cell culture and DNA transfection

EB cells, EB-1 cells and MEFs have been described elsewhere[7,18,19]. All cancer cell lines were from American type culture collection (ATCC). The conditions for cell culture are described in Supplementary Information. LipofectAMINE reagent (Gibco) was used for transient and stable transfection of cells, according to the manufacturer's protocol. For selecting stable clones, transfected cells were grown in medium containing 400 $\mu g\,ml^{-1}$ G418 for neomycin resistance, or 2 $\mu g\,ml^{-1}$ hygromycin B for hygromycin resistance.

Northern, western and cell cycle analyses

Total RNA was isolated from growing cells using TRIzol reagent (Gibco). Poly(A)$^+$ RNA was purified using a olyATtract mRNA isolation system (Promega), according to the manufacturer's instructions. The experimental procedures for northern, western and cell cycle analyses are described in Supplementary Information.

Luciferase reporters, PAC1 siRNA and PAC1 expression plasmids

The regulatory and promoter region of the human *PAC1* gene was cloned by PCR from normal human genomic DNA using corresponding primers based on the human genome database. PCR products were subcloned into a pT–Adv vector (Clontech) for sequencing and compared with the genome database. The PAC1 promoter was subcloned into the pGL3-basic reporter (Promega). The deletion of the palindrome in PAC1 of the pGL3-PAC1-711 plasmid was generated using the QuickChange site-directed mutagenesis kit (Stratagene) according to the manufacturer's protocol. The designs for the constructs, luciferase assay, cellular viability and TdT-mediated dUTP nick end labelling (TUNEL) assay are described in Supplementary Information.

DNase I footprinting analysis

The human PAC1 promoter was end-labelled with [γ-^{32}P]ATP by T4 polynucleotide kinase, digested with *Eco*RV and purified to obtain the sense strand 3′-end-labelled probe, and subjected to DNaseI footprinting analysis with the Core Footprinting System (Promega), according to the manufacturer's instructions. Recombinant p53 protein was produced in insect cells infected with a baculovirus vector expressing human wild-type p53, and partially purified through affinity chromatography. The purified recombinant p53 protein was added to bind to radiolabelled probe fragment ($1–2 \times 10^4$ c.p.m.) at 37 °C for 30 min, followed by the addition of DNase I. Samples were subjected to polyacrylamide gel electrophoresis (PAGE) under denaturing conditions and the dried gel was exposed to autoradiography with an intensifying screen.

Electrophoretic mobility shift assay

Synthetic oligonucleotides (pairs of sense and antisense) were annealed and labelled with ^{32}P by using T4 polynucleotide kinase and [γ-^{32}P]ATP, as described elsewhere[20]. Briefly, ^{32}P-labelled probes were mixed with purified recombinant p53 in a 20-μl DNA binding reaction buffer. For specificity or competition controls, a labelled random oligonucleotide or excess of unlabelled corresponding oligonucleotide were added together in reactions. For supershift, the anti-p53 monoclonal antibodies (PAb421, PAb1801; Oncogene) were included. The reaction mixtures were incubated at 4 °C for 20 min, resolved by a 4% polyacrylamide gel, and exposed for photography.

Anchorage-independent growth and tumorigenicity assays

Exponentially growing cells (6×10^3 cells per group) were mixed with 3 ml top agarose containing 0.35% low melting point agarose in MEM medium with 10% fetal bovine serum (FBS), and seeded onto 3 ml 0.6% solidified agarose in the same medium in six-well plates. Colonies with a diameter of >1.0 mm were counted after two weeks of incubation. Results are expressed as means of colony number ± s.d. of triplicate repeats. For tumorigenicity assay *in vivo*, 4-week-old athymic nude mice (BALB/c/nu/nu, Harlan–Sprague–Dawley) were inoculated subcutaneously with 5×10^5 cells in 0.2 ml MEM medium. Tumour volume was determined by the equation $V = (L \times W^2) \times 0.5$, where L is length and W is width of tumour. Values are the means ± s.d. of the counted tumours.

Received 17 December 2002; accepted 20 February 2003; doi:10.1038/nature01519.

1. Levine, A. J. p53, the cellular gatekeeper for growth and division. *Cell* **88,** 323–331 (1997).
2. Vogelstein, B., Lane, D. & Levine, A. J. Surfing the p53 network. *Nature* **408,** 307–310 (2000).
3. Rohan, P. J. *et al.* PAC-1: a mitogen-induced nuclear protein tyrosine phosphatase. *Science* **259,** 1763–1766 (1993).
4. Ward, Y. *et al.* Control of MAP kinase activation by the mitogen-induced threonine/tyrosine phosphatase PAC1. *Nature* **367,** 651–654 (1994).
5. Kastan, M. B. *et al.* A mammalian cell cycle checkpoint pathway utilizing p53 and GADD45 is defective in ataxia-telangiectasia. *Cell* **71,** 587–597 (1992).
6. Brugarolas, J. *et al.* Radiation-induced cell cycle arrest compromised by p21 deficiency. *Nature* **377,** 552–557 (1995).
7. Zhao, R. *et al.* Analysis of p53-regulated gene expression patterns using oligonucleotide arrays. *Genes Dev.* **14,** 981–993 (2000).
8. Nishida, E. & Gotoh, Y. The MAP kinase cascade is essential for diverse signal transduction pathways. *Trends Biochem. Sci.* **18,** 128–131 (1993).
9. Shaw, P. *et al.* Induction of apoptosis by wild-type p53 in a human colon tumour-derived cell line. *Proc. Natl Acad. Sci. USA* **89,** 4495–4499 (1992).
10. Yin, Y., Solomon, G., Deng, C. & Barrett, J. C. Differential regulation of p21 by p53 and Rb in cellular response to oxidative stress. *Mol. Carcinog.* **24,** 15–24 (1999).
11. El Deiry, W. S., Kern, S. E., Pietenpol, J. A., Kinzler, K. W. & Vogelstein, B. Definition of a consensus binding site for p53. *Nature Genet* **1,** 45–49 (1992).
12. Baker, S. J., Markowitz, S., Fearon, E. R., Willson, J. K. & Vogelstein, B. Suppression of human colorectal carcinoma cell growth by wild-type p53. *Science* **249,** 912–915 (1990).
13. Foord, O. S., Bhattacharya, P., Reich, Z. & Rotter, V. A DNA binding domain is contained in the C-terminus of wild type p53 protein. *Nucleic Acids Res.* **19,** 5191–5198 (1991).
14. Gu, W. & Roeder, R. G. Activation of p53 sequence-specific DNA binding by acetylation of the p53 C-terminal domain. *Cell* **90,** 595–606 (1997).
15. El-Deiry, W. S. *et al.* Topological control of p21WAF1/CIP1 expression in normal and neoplastic tissues. *Cancer Res.* **55,** 2910–2919 (1995).
16. Fire, A. *et al.* Potent and specific genetic interference by double-stranded RNA in *Caenorhabditis elegans*. *Nature* **391,** 806–811 (1998).
17. Suit, G. *et al.* A DNA vector-based RNAi technology to suppress gene expression in mammalian cells. *Proc. Natl Acad. Sci. USA* **99,** 5515–5520 (2002).
18. Almasan, A. *et al.* Deficiency of retinoblastoma protein leads to inappropriate S-phase entry, activation of E2F-responsive genes, and apoptosis. *Proc. Natl Acad. Sci. USA* **92,** 5436–5440 (1995).
19. Yin, Y. *et al.* Involvement of p85 in p53-dependent apoptotic response to oxidative stress. *Nature* **391,** 707–710 (1998).
20. Maiyar, A. C., Huang, A. J., Phu, P. T., Cha, H. H. & Firestone, G. L. p53 stimulates promoter activity of the sgk. serum/glucocorticoid-inducible serine/threonine protein kinase gene in rodent mammary epithelial cells. *J. Biol. Chem.* **271,** 12414–12422 (1996).
21. Minden, A. *et al.* c-Jun N-terminal phosphorylation correlates with activation of the JNK subgroup but not the ERK subgroup of mitogen-activated protein kinases. *Mol. Cell. Biol.* **14,** 6683–6688 (1994).

Supplementary Information accompanies the paper on *Nature*'s website (http://www.nature.com/nature).

Acknowledgements We thank A. J. Levine for advice on promoter studies and for providing critical reagents, and W. Gu for the pCMV-p53Δ270 plasmid. We are grateful to H. B. Lieberman for critical reading of the manuscript. We also thank T. A. Sato for help with the luciferase assay. This work was supported by a start up fund from the Columbia University (Y.Y.) and NIH grants (to Y.Y. and E.J.H).

Competing interests statement The authors declare that they have no competing financial interests.

Correspondence and requests for materials should be addressed to Y.Y. (e-mail: yy151@columbia.edu).

The voltage dependence of NADPH oxidase reveals why phagocytes need proton channels

Thomas E. DeCoursey, Deri Morgan & Vladimir V. Cherny

Department of Molecular Biophysics and Physiology, Rush Presbyterian St Luke's Medical Center, 1750 West Harrison, Chicago, Illinois 60612, USA

The enzyme NADPH oxidase in phagocytes is important in the body's defence against microbes: it produces superoxide anions (O_2^-, precursors to bactericidal reactive oxygen species[1]). Electrons move from intracellular NADPH, across a chain comprising FAD (flavin adenine dinucleotide) and two haems, to reduce extracellular O_2 to O_2^-. NADPH oxidase is electrogenic[2], generating electron current (I_e) that is measurable under voltage-clamp conditions[3,4]. Here we report the complete current–voltage relationship of NADPH oxidase, the first such measurement of a plasma membrane electron transporter. We find that I_e is voltage-independent from −100 mV to >0 mV, but is steeply inhibited by further depolarization, and is abolished at about +190 mV. It was proposed that H^+ efflux[2] mediated by voltage-gated proton channels[5,6] compensates I_e, because Zn^{2+} and Cd^{2+} inhibit both H^+ currents[7–9] and O_2^- production[10]. Here we show that COS-7 cells transfected with four NADPH oxidase

components[11], but lacking H^+ channels[12], produce O_2^- in the presence of Zn^{2+} concentrations that inhibit O_2^- production in neutrophils and eosinophils. Zn^{2+} does not inhibit NADPH oxidase directly, but through effects on H^+ channels. H^+ channels optimize NADPH oxidase function by preventing membrane depolarization to inhibitory voltages.

Because it is electrogenic, NADPH oxidase ought to be sensitive to membrane potential. However, this property has been demonstrated only over a limited voltage range[3,13]. Furthermore, the hypothesis that voltage-gated proton channels compensate most of the charge generated by NADPH oxidase function[2,5,6,14] has not been tested directly, and recently, K^+ was proposed to have a similar role[15]. Although Zn^{2+} or Cd^{2+} can inhibit O_2^- production[10,16], they do so at higher concentrations than are required to inhibit voltage-gated proton currents[5,9,17], raising the possibility that these metals directly inhibit NADPH oxidase or affect other processes. Here we establish the importance of H^+ currents, and show that the voltage dependence of NADPH oxidase optimizes its performance.

The current–voltage relationship of I_e generated by NADPH oxidase is shown in Fig. 1. Eosinophils in permeabilized-patch configuration[4,17] were stimulated with the potent respiratory burst agonist, PMA (phorbol myristate acetate), which activates NADPH oxidase, resulting in inward I_e (ref. 17). We isolated I_e by its sensitivity to the NADPH oxidase inhibitor diphenylene iodinium chloride (DPI)[18]. Voltage-gated proton currents were inhibited by addition of 1.5–6.0 mM $ZnCl_2$ to the bathing solution. These high concentrations of $ZnCl_2$ (free Zn^{2+}, 0.5–5.0 mM) did not reduce I_e noticeably. The mean reduction of I_e by 3 mM Zn^{2+} was 5.9 ± 6.5% (mean ± s.e.m., $n = 6$), ruling out direct inhibition of NADPH oxidase. Therefore, inhibition of O_2^- production by high Zn^{2+} concentrations in previous studies[10,19] was not due to direct inhibition of NADPH oxidase. We compared currents elicited by voltage ramps soon after DPI addition (before inhibition was evident) and later (Fig. 1a, filled squares and open circles, respectively). Full inhibition of I_e by DPI takes 1–2 min (ref. 13). The net DPI-sensitive I_e is plotted in Fig. 1b. The similarity of I_e measured during ramps (open triangles) and at constant voltage (filled circles) confirms that I_e reached steady state at each voltage during the ramps. This result is expected because the turnover rate of NADPH oxidase is ~300 s^{-1} (ref. 20).

I_e–V relationships measured in four cells (of ten studied) are plotted in Fig. 1c to illustrate the variability of the data. The expected inhibition of electron efflux by depolarization occurs only at large positive voltages, where the I_e–V relationship becomes steeply voltage dependent. Electron transport was abolished at +165 to +220 mV (+188 ± 19 mV; mean ± s.d., $n = 10$). The standard redox potential of the NADPH/$NADP^+$ pair is −320 mV (ref. 21) and that of O_2/O_2^- is −160 mV (ref. 22). Thus, the nominal driving force for electron movement across the chain is +160 mV, although this pseudo-equilibrium potential ought to depend on concentration[23]. Depolarization of the phagocyte membrane to the equilibrium potential of the electron transport pathway shuts down NADPH oxidase. The I_e–V relationship was surprisingly independent of voltage from −100 mV to an inflection point that occurred between 0 mV and +80 mV. In some cells there was weak voltage dependence at negative voltages (for example, open symbols in Fig. 1c), but strong rectification of the I_e–V relationship was observed consistently. Evidently, a voltage-independent process is rate limiting at voltages <0 mV, and a voltage-sensitive process becomes rate determining only during extreme depolarization. Electron transfer between the two intramembrane haem groups in $gp91^{phox}$ (ref. 24) is a likely candidate for this voltage sensitive process.

If no compensatory mechanism existed, I_e in an eosinophil at 37 °C would depolarize the membrane by ~1 kV min^{-1} during the respiratory burst, driving the membrane from its resting potential of −60 mV (ref. 25) to +190 mV in <20 ms, and O_2^- production would cease. For continuous function of NADPH oxidase, this charge movement must be balanced by an efficient mechanism that responds rapidly to depolarization. Voltage-gated proton channels are ideally suited to this task, because they are activated by cytosolic acidification and depolarization[5,8,17,26]. Depolarization to +20 mV activates sufficient outward H^+ current to compensate I_e completely in a PMA-stimulated eosinophil[17]. However, the only evidence supporting this role is the inhibition of O_2^- production by Cd^{2+}

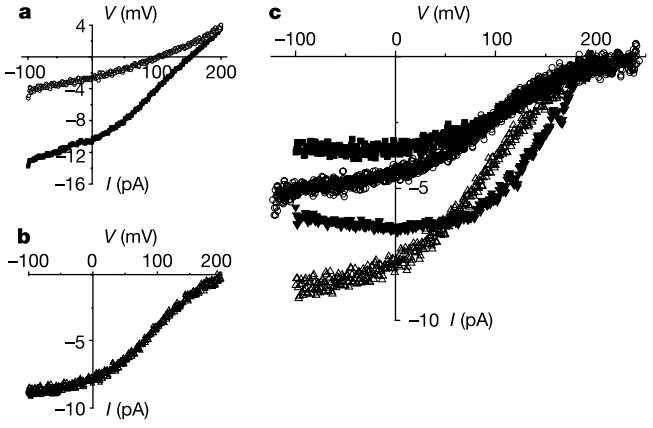

Figure 1 Current–voltage relationship for NADPH-oxidase-mediated electron current (I_e) in human eosinophils. **a**, Uncorrected averaged currents recorded in an eosinophil during voltage ramps early (filled squares) and late (open circles) after addition of DPI to a cell that was previously stimulated with 60 nM PMA. Voltage ramps were applied at 5-s intervals from −100 mV to +200 mV. The membrane was held at −60 mV after each ramp, and stepped to −100 mV for 400 ms before the start of the ramp. To inhibit H^+ channels, 5 mM $ZnCl_2$ was added to all bath solutions. The average of three ramp currents recorded ~4 min after DPI was added was subtracted point-by-point from the average of four records obtained within 20 s after DPI addition. The difference (**b**) is DPI-sensitive I_e. Filled symbols indicate 'steady-state' net I_e measured at the end of the 400-ms prepulse to −100 mV and after 4.4 s at −60 mV. **c**, Net I_e in four eosinophils representative of the variability observed in I_e–V relationships in ten cells.

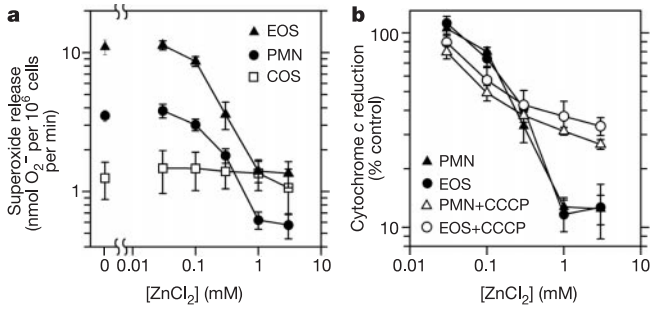

Figure 2 Factors affecting superoxide production. **a**, Sensitivity of the maximum rate of superoxide production to $ZnCl_2$ in human eosinophils (EOS, filled triangles), neutrophils (PMN, filled circles) and COS_{phox} cells (COS, open squares) (mean ± s.e.m. of 4, 9 or 6 experiments, respectively). Release of O_2^- at 37 °C was quantified by reduction of cytochrome *c* as described previously[17], except that cells were suspended in Ringer's solution to avoid chelation of Zn^{2+}. Inhibition was significant at [$ZnCl_2$] ≥ 0.3 mM ($P < 0.01$, Student's unpaired *t*-test). **b**, Restoration of O_2^- production (mean and s.e.m.) by 60 μM CCCP (open symbols), in human eosinophils (EOS, filled triangles, $n = 3$) or neutrophils (PMN, filled circles, $n = 4$) inhibited by Zn^{2+}. For both cell types, O_2^- production at 1 or 3 mM $ZnCl_2$ was significantly greater in the presence of CCCP ($P < 0.05$). CCCP alone appeared to partially inhibit O_2^- release, perhaps by uncoupling mitochondria, although this was not statistically significant. The control data are a subset of the data in **a**. All values are normalized to those in the absence of Zn^{2+}.

and Zn^{2+} (ref. 10) at concentrations larger than those needed to inhibit voltage-gated proton current[9,16]. If Zn^{2+} inhibits O_2^- production by inhibiting H^+ currents, then it should not affect O_2^- production in cells that do not express voltage-gated proton channels. The only cells known to lack H^+ channels are COS-7 cells[12]. Therefore, we studied O_2^- production in COS-7 cells transfected with the four main NADPH oxidase components, $gp91^{phox}$, $p47^{phox}$, $p67^{phox}$ and $p22^{phox}$, which we call COS_{phox} cells[11,12]. In Fig. 2 the concentration–response relationship for $ZnCl_2$ inhibition of the maximal rate of O_2^- production is compared in human eosinophils (filled triangles), neutrophils (filled circles) and COS_{phox} cells (open squares) stimulated with 60 nM PMA. O_2^- generation was measured by a standard cytochrome *c* reduction assay[17]. There was little effect of up to 3 mM $ZnCl_2$ on COS_{phox} cells, which lack H^+ channels. In contrast, 0.1–0.3 mM $ZnCl_2$ clearly reduced O_2^- production in human phagocytes, with nearly complete inhibition at 3 mM $ZnCl_2$. Evidently, $ZnCl_2$ reduces O_2^- production by inhibiting voltage-gated proton channels, and cannot do so in cells that lack H^+ channels. The charge-compensating mechanism of COS_{phox} cells is not known, but it evidently is less sensitive to Zn^{2+} than are H^+ channels. Figure 2b illustrates that the inhibition of O_2^- production in phagocytes by Zn^{2+} was partially overcome by addition of the protonophore, CCCP (carbonyl cyanide *m*-chlorophenylhydrazone). In contrast, the K^+ ionophore, valinomycin, exacerbates the inhibition of O_2^- production by Cd^{2+} or Zn^{2+} (refs 6, 10). Together, these results indicate that proton efflux rather than flux of another ion compensates for charge separation by NADPH oxidase in phagocytes.

A small fraction of I_e might be compensated by K^+, as was proposed recently[15]. However, we rule out significant involvement of K^+ current in compensating charge. First, although unstimulated eosinophils have inwardly rectifying K^+ channels, they have no outward K^+ conductance, and blocking the inward rectifier does not compromise O_2^- production[27]. In PMA-stimulated eosinophils in which I_e attests to NADPH oxidase activity, we do not detect outward K^+ currents (data not shown). Furthermore, upon stimulation by PMA, the membrane potential of eosinophils depolarizes to the Nernst potential for H^+ over a wide range of pH gradients[28], demonstrating that the predominant conductance is proton selective. Thus, H^+ efflux compensates most of the charge separation by NADPH oxidase in active phagocytes. Although any K^+ efflux would contribute to charge compensation, the primary role of K^+ efflux is regulation of the phagosomal volume, ionic strength and pH (ref. 15). K^+ efflux, in contrast to H^+ efflux, causes osmotic and pH changes in the phagosome, which promote activity of proteolytic enzymes[15]. Similarly, complete depletion of phagosomal Cl^- by flux into cytosol would compensate less than 4% of the charge translocated by NADPH during the respiratory burst[15]. Proton flux is ideally suited to charge compensation, because it is osmotically neutral and pH neutral.

Voltage-gated proton channels are highly sensitive to divalent cations[7–9], with significant inhibition by 1 μM $ZnCl_2$ at pH ≥ 7 in eosinophils[17]. Paradoxically, much higher concentrations are required to inhibit O_2^- production. The I_e–V relationship reported here explains this apparent discrepancy. Zn^{2+} and Cd^{2+} do not 'block' H^+ channels by steric occlusion, but rather shift H^+ current activation to more positive voltages[5,9,26]. Because I_e is voltage independent from the normal resting potential to beyond 0 mV (Fig. 1), shifting the threshold for H^+ current activation within this voltage range does not inhibit NADPH oxidase. Analogously, depolarization to ~0 mV with high K^+ concentration had no effect on O_2^- production by eosinophils[27], and only partially inhibited O_2^- production by neutrophils[29]. Distinct inhibition of O_2^- production in neutrophils first occurred at 100–300 μM Zn^{2+} (Fig. 2), which would shift the threshold for activating H^+ channels at pH 7.4 by 80–90 mV (ref. 9); that is, from −20 mV in activated phagocytes[4] to +60 to +70 mV. Consequently, activation of sufficient H^+ efflux to compensate I_e would occur only at voltages within the range where I_e is inhibited directly by voltage. In conclusion, Zn^{2+} inhibits O_2^- production by shifting H^+ channel activation into or beyond the voltage-dependent region of the I_e–V relationship.

During the respiratory burst in neutrophils, the membrane depolarizes to +58 mV (ref. 30), which is close to the point at which depolarization begins to inhibit I_e. However, in spite of this depolarization of >100 mV from the resting potential, there is minimal 'self-inhibition', because I_e is practically voltage independent throughout this voltage range. The average reduction of I_e at +58 mV, relative to I_e at the 'resting potential' of −60 mV, was only 24 ± 15% (mean ± s.d., $n = 10$). The surprisingly large range over which NADPH oxidase is insensitive to membrane potential provides a safety factor that ensures optimal function of this enzyme unless it is confronted by drastic membrane depolarization. The depolarization that occurs during the respiratory burst is sufficient to activate compensatory H^+ efflux through H^+ channels without significantly inhibiting the NADPH oxidase. □

Methods

Eosinophil and neutrophil isolation

Venous blood was drawn from healthy adult volunteers under informed consent, as approved by our Institutional Review Board and in accordance with Federal regulations. Neutrophils were isolated by density-gradient centrifugation[17], and were suspended in 10 mM HEPES-buffered HBSS (with Ca^{2+} and Mg^{2+}) at pH 7.4 for O_2^- measurements. Eosinophils were isolated from the neutrophils by negative selection using anti-CD16 immunomagnetic beads[17]. Patch-clamp studies were done on freshly isolated eosinophils, and on eosinophils incubated overnight at 37 °C in RPMI 1640 medium containing 25 mM HEPES and L-glutamine (Gibco), supplemented with 10% fetal bovine serum (Bio-Whittaker), 100 units ml^{-1} penicillin, 100 μg ml^{-1} streptomycin (Sigma), and 1 ng ml^{-1} recombinant human GM-CSF (R & D Systems). Cells were provided by Larry L. Thomas.

COS_{phox} cells

COS-7 cells stably transfected with the four main subunits of NADPH oxidase—$gp91^{phox}$, $p22^{phox}$, $p47^{phox}$ and $p67^{phox}$ (COS_{phox} cells)—were developed by Price *et al.*[11] and were provided by M. Dinauer. COS_{phox} cells were maintained in suspension as described[12].

Electrophysiology

For permeabilized-patch recording, the pipette solutions contained 80 mM KCH_3SO_3 or 100 mM tetramethylammonium methanesulphonate, 50 mM NH_4^+ in the form of 25 mM $(NH_4)_2SO_4$, 2 mM $MgCl_2$, 5 mM BES, 1 mM EGTA, titrated to pH 7.0, and ~500 μg ml^{-1} solubilized amphotericin B (Sigma). The symmetrical 50 mM NH_4^+ gradient 'clamped' the intracellular pH to extracellular pH (ref. 4). The bath solution was identical to the 100 mM tetramethylammonium methanesulphonate pipette solution, but lacked amphotericin B. Studies were done at 20–25 °C. PMA and CCCP were obtained from Sigma. Other details of electrophysiological measurements are described elsewhere[17].

Received 14 October 2002; accepted 25 February 2003; doi:10.1038/nature01523.

1. Babior, B. M. NADPH oxidase: an update. *Blood* **93,** 1464–1476 (1999).
2. Henderson, L. M., Chappell, J. B. & Jones, O. T. The superoxide-generating NADPH oxidase of human neutrophils is electrogenic and associated with an H^+ channel. *Biochem. J.* **246,** 325–329 (1987).
3. Schrenzel, J. *et al.* Electron currents generated by the human phagocyte NADPH oxidase. *Nature* **392,** 734–737 (1998).
4. DeCoursey, T. E., Cherny, V. V., Zhou, W. & Thomas, L. L. Simultaneous activation of NADPH oxidase-related proton and electron currents in human neutrophils. *Proc. Natl Acad. Sci. USA* **97,** 6885–6889 (2000).
5. DeCoursey, T. E. & Cherny, V. V. Potential, pH, and arachidonate gate hydrogen ion currents in human neutrophils. *Biophys. J.* **65,** 1590–1598 (1993).
6. Henderson, L. M., Chappell, J. B. & Jones, O. T. Internal pH changes associated with the activity of NADPH oxidase of human neutrophils. Further evidence for the presence of an H^+ conducting channel. *Biochem. J.* **251,** 563–567 (1988).
7. Mahaut-Smith, M. The effect of zinc on calcium and hydrogen ion currents in intact snail neurones. *J. Exp. Biol.* **145,** 455–469 (1989).
8. Thomas, R. C. & Meech, R. W. Hydrogen ion currents and intracellular pH in depolarized voltage-clamped snail neurones. *Nature* **299,** 826–828 (1982).
9. Cherny, V. V. & DeCoursey, T. E. pH-dependent inhibition of voltage-gated H^+ currents in rat alveolar epithelial cells by Zn^{2+} and other divalent cations. *J. Gen. Physiol.* **114,** 819–838 (1999).
10. Henderson, L. M., Chappell, J. B. & Jones, O. T. Superoxide generation by the electrogenic NADPH oxidase of human neutrophils is limited by the movement of a compensating charge. *Biochem. J.* **255,** 285–290 (1988).
11. Price, M. O. *et al.* Creation of a genetic system for analysis of the phagocyte respiratory burst: high-level reconstitution of the NADPH oxidase in a nonhematopoietic system. *Blood* **99,** 2653–2661 (2002).
12. Morgan, D., Cherny, V. V., Price, M. O., Dinauer, M. C. & DeCoursey, T. E. Absence of proton channels in COS-7 cells expressing functional NADPH oxidase components. *J. Gen. Physiol.* **119,** 571–580 (2002).

13. Cherny, V. V., Henderson, L. M., Xu, W., Thomas, L. L. & DeCoursey, T. E. Activation of NADPH oxidase-related proton and electron currents in human eosinophils by arachidonic acid. *J. Physiol. (Lond.)* **535,** 783–794 (2001).
14. Nanda, A. & Grinstein, S. Protein kinase C activates an H^+ (equivalent) conductance in the plasma membrane of human neutrophils. *Proc. Natl Acad. Sci. USA* **88,** 10816–10820 (1991).
15. Reeves, E. P. *et al.* Killing activity of neutrophils is mediated through activation of proteases by K^+ flux. *Nature* **416,** 291–297 (2002).
16. Kapus, A., Szászi, K. & Ligeti, E. Phorbol 12-myristate 13-acetate activates an electrogenic H^+-conducting pathway in the membrane of neutrophils. *Biochem. J.* **281,** 697–701 (1992).
17. DeCoursey, T. E., Cherny, V. V., DeCoursey, A. G., Xu, W. & Thomas, L. L. Interactions between NADPH oxidase-related proton and electron currents in human eosinophils. *J. Physiol. (Lond.)* **535,** 767–781 (2001).
18. Cross, A. R. & Jones, O. T. The effect of the inhibitor diphenylene iodonium on the superoxide-generating system of neutrophils. Specific labelling of a component polypeptide of the oxidase. *Biochem. J.* **237,** 111–116 (1986).
19. Lowenthal, A. & Levy, R. Essential requirement of cytosolic phospholipase A_2 for activation of the H^+ channel in phagocyte-like cells. *J. Biol. Chem.* **274,** 21603–21608 (1999).
20. Koshkin, V., Lotan, O. & Pick, E. Electron transfer in the superoxide-generating NADPH oxidase complex reconstituted *in vitro*. *Biochim. Biophys. Acta* **1319,** 139–146 (1997).
21. Burton, K. & Wilson, T. H. The free-energy changes for the reduction of diphosphopyridine nucleotide and the dehydrogenation of L-malate and L-glycerol 1-phosphate. *Biochem. J.* **54,** 86–94 (1953).
22. Wood, P. M. The redox potential of the system oxygen-superoxide. *FEBS Lett.* **44,** 22–24 (1974).
23. Läuger, P. *Electrogenic Ion Pumps* (Sinauer Associates, Sunderland, Massachusetts, 1991).
24. Biberstine-Kinkade, K. J. *et al.* Heme-ligating histidines in flavocytochrome b_{558}: identification of specific histidines in $gp91^{phox}$. *J. Biol. Chem.* **276,** 31105–31112 (2001).
25. Gordienko, D. V. *et al.* Voltage-activated proton current in eosinophils from human blood. *J. Physiol. (Lond.)* **496,** 299–316 (1996).
26. Byerly, L., Meech, R. & Moody, W. Rapidly activating hydrogen ion currents in perfused neurones of the snail, *Lymnaea stagnalis*. *J. Physiol. (Lond.)* **351,** 199–216 (1984).
27. Tare, M. *et al.* Inwardly rectifying whole cell potassium current in human blood eosinophils. *J. Physiol. (Lond.)* **506,** 303–318 (1998).
28. Bánfi, B. *et al.* A novel H^+ conductance in eosinophils: unique characteristics and absence in chronic granulomatous disease. *J. Exp. Med.* **190,** 183–194 (1999).
29. Martin, M. A., Nauseef, W. M. & Clark, R. A. Depolarization blunts the oxidative burst of human neutrophils. Parallel effects of monoclonal antibodies, depolarizing buffers, and glycolytic inhibitors. *J. Immunol.* **140,** 3928–3935 (1988).
30. Jankowski, A. & Grinstein, S. A noninvasive fluorimetric procedure for measurement of membrane potential. Quantification of the NADPH oxidase-induced depolarization in activated neutrophils. *J. Biol. Chem.* **274,** 26098–26104 (1999).

Acknowledgements We thank A. R. Cross and L. L. Thomas for discussions, and T. Iastrebova and J. Murphy for technical assistance. This work was supported in part by the Heart, Lung and Blood Institute of the National Institutes of Health (T.E.D.).

Competing interests statement The authors declare that they have no competing financial interests.

Correspondence and requests for materials should be addressed to T.E.D. (e-mail: tdecours@rush.edu).

Crystal structure of a transcription factor IIIB core interface ternary complex

Z. Sean Juo*, George A. Kassavetis†, Jimin Wang*, E. Peter Geiduschek† & Paul B. Sigler*‡

** Department of Molecular Biophysics & Biochemistry, Yale University, 266 Whitney Avenue, New Haven, Connecticut 06520-8114, USA*
† Center for Molecular Genetics, University of California, San Diego, 9500 Gilman Drive, La Jolla, California 92093-0634, USA
‡ Deceased

Transcription factor IIIB (TFIIIB), consisting of the TATA-binding protein (TBP), TFIIB-related factor (Brf1) and Bdp1, is a central component in basal and regulated transcription by RNA polymerase III[1–4]. TFIIIB recruits its polymerase to the promoter and subsequently has an essential role in the formation of the open initiation complex. The amino-terminal half of Brf1 shares a high degree of sequence similarity with the polymerase II general transcription factor TFIIB, but it is the carboxy-terminal half of Brf1 that contributes most of its binding affinity with TBP[5–8]. The principal anchoring region is located between residues 435 and 545 of yeast Brf1, comprising its homology domain II. The same region also provides the primary interface for assembling Bdp1 into the TFIIIB complex[9]. We report here a 2.95 Å resolution crystal structure of the ternary complex containing Brf1 homology domain II, the conserved region of TBP and 19 base pairs of U6 promoter DNA. The structure reveals the core interface for assembly of TFIIIB and demonstrates how the loosely packed Brf1 domain achieves remarkable binding specificity with the convex and lateral surfaces of TBP.

The crystal structure of the Brf1–TBP–DNA ternary complex is shown in Fig. 1. The revealed portion of Brf1 (residues 437–506) extends in parallel with helices H2 and H2′ across the convex surface of TBP. After two nearly 90° turns, the remaining polypeptide positions itself along the lateral surface of the first structural repeat of TBP (Fig. 2a, b). This 'vine-on-a-tree' conformation is substantially different from previously reported polymerase (pol) II transcription ternary complexes involving TBP and DNA[10]. The structure also demonstrates that the convex surface of TBP is extensively engaged as the principal interface for binding. A total of 31 Brf1 residues in the crystal structure interact with 29 TBP residues through 31 hydrogen bonds and 114 van der Waals contacts. The large number of interactions is exceptional, approximately three to five times greater than for the comparable pol II ternary complex structures. As a result of all these contacts, 3,230 $Å^2$ of TBP surface area becomes inaccessible to solvent on Brf1 binding.

The conformation of Brf1 homology domain II revealed in the crystal structure is unusually extended, which does not fit the general idea of a structural domain. Given that this Brf1 segment, when unbound, is resistant to protease digestion (Z.S.J., unpublished results), it must adopt a stable structural fold in solution and undergo global unfolding on complex formation with TBP. This resembles the maintenance of a partially unfolded state of the GTPase-activating protein SptP by its cognate chaperone SicP, as the latter stabilizes the elongated helical conformation of the target protein[11]. The revealed Brf1 domain does not involve DNA binding in the crystal structure. Notably, the unresolved segment (residues 507–596) contains a proposed cryptic DNA-binding domain[12]. The H25 helix of Brf1 lies close to DNA and its trajectory points towards the start site of transcription, which is consistent with the DNA-binding potential of this segment.

The conformation of DNA-bound TBP remains similar to the related pol II ternary complex structures[10], with an average root-mean-square (r.m.s.) deviation of 0.54 Å for Cα positions despite variations of sequence. In comparison with the apo-structure[13], TBP undergoes noticeable conformational changes on DNA binding (averaged r.m.s. deviation of 1.19 Å for Cα positions). The two direct repeats move slightly closer to accommodate the widened narrow groove of the TATA element, and an approximately 3.3 Å displacement is observed at the first stirrup region of TBP when its second structural repeat is aligned. Owing to the pseudo-symmetrical nature of the yeast U6 TATA motif, its sequence for crystallization was modified to favour unidirectional binding of TBP[14] (Fig. 2c). As observed previously, the TATA element is smoothly curved and doubly kinked at the termini. The minor groove width of the downstream B-form DNA is substantially narrower, which is a consequence of being predominantly (A + T)-rich. It is worth noting that the terminal A-tract segment interacts firmly with its non-crystallographic symmetry (NCS) counterpart (see Supplementary Information). Given that 20 base pairs of DNA stack between two complexes and maintain a stable conformation without any external support, the stiffness of A-tract sequence must contribute significantly to maintaining local structural stability in the crystal lattice[14].

The Brf1 homology domain II is mainly helical. The existence of four helices (H21, H23, H24 and H25) is consistent with secondary

